Acid number, viscosity and end-point detection in a multiphase high temperature polymerisation process using an online miniaturised MEMS Fabry-Pérot Interferometer

Authors:

Claudio Avila *†, Christos Mantzaridis ‡, Joan Ferré §, Rodrigo Rocha de Oliveira ‖, Uula Kantojärvi ⊥, Anna Rissanen #, Poppy Krassa ‡, Anna de Juan Capdevila ‖, Frans L. Muller †, Timothy N. Hunter †, and Richard A. Bourne *†

Affiliation and address:

† School of Chemical and Process Engineering, University of Leeds, Leeds LS2 9JT, United Kingdom

‡ Megara Resins, 38th km New National Rd. Athens-Corinth, Megara 191 00, Greece

§ Department of Analytical Chemistry and Organic Chemistry, Universitat Rovira i Virgili, Tarragona 43007, Spain

‖ Department of Chemical Engineering and Analytical Chemistry, Universitat de Barcelona, Barcelona 08028, Spain

⊥ Spectral Engines Oy, Kutomotie 16, Helsinki, Finland

VTT Technical Research Centre of Finland, Tietotie 3, Espoo, Finland

Author email address

Claudio Avila: C.R.Avila@leeds.ac.uk

Christos Mantzaridis: cmantzaridis@gmail.com

Joan Ferré: joan.ferre@urv.cat

Rodrigo Rocha de Oliveira: rrochade10@alumnes.ub.edu
Uula Kantojärvi: uula@spectralengines.com
Anna Rissanen: Anna.Rissanen@vtt.fi
Poppy Krassa: p.krassa@megararesins.com
Anna de Juan Capdevila: anna.dejuan@ub.edu
Frans L. Muller: F.L.Muller@leeds.ac.uk
Timothy N. Hunter: T.N.Hunter@leeds.ac.uk
Richard A. Bourne: R.A.Bourne@leeds.ac.uk

Highlights

- The application of online near infrared MEMS sensor used to monitor progress in extreme multiphase and high temperature process conditions
- PLS models generated for acid number and viscosity, and MSPC model for detecting reaction end-point of industrial polyester synthesis
- MEMS-FPI sensor demonstrated to be a robust and cost effective alternative for sampling and offline testing

Abstract:

Recent advances in the latest generation of MEMS (micro-electro-mechanical system) Fabry-Pérot interferometers (FPI) for near infrared (NIR) wavelengths has led to the development of ultra-fast and low cost NIR sensors with potential to be used by the process industry. One of these miniaturised sensors operating from 1350 to 1650 nm, was integrated into a software platform to monitor a multiphase gas-liquid process for production of saturated polyester

resins. Twelve batches were run in a two litre reactor mimicking industrial conditions (24 hr process, with temperatures ranging from 220-240 °C), using an immersion NIR transmission probe. Because of the multiphase nature of the reaction fluids strong interference produced by process disturbances such as temperature variations and the presence of solid particles and bubbles in the online spectra required a robust pre-processing algorithms and a good long-term stability of the probe. These allowed partial least squares (PLS) regression models to be built for the key analytical parameters acid number and viscosity. In parallel, spectra were also used to build an end-point detection model based on principal component analysis (PCA) for multivariate statistical process control (MSPC). The novel MEMS-FPI sensor combined with robust chemometric analysis proved to be a suitable and affordable alternative for online process monitoring, contributing to sustainability in the process industry.

Keywords

Near infrared spectroscopy; MEMS Fabry-Pérot interferometer; online process monitoring; high temperature polymerisation; saturated polyester resin; chemometrics

1. Introduction

The production of saturated polyester resins is a process of global relevance, with large production volumes and a considerable environmental footprint [1]. These are condensation polymers, normally formed in a polycondensation reaction between polycarboxylic acids or their anhydrides and polyalcohols, producing water as a by-product. This is a reversible equilibrium reaction, industrially performed between 220-240 °C, where the formation of polyester is promoted when water and low boiling point products are distilled out [2]. The composition of the polyester resin is critically important in achieving the balance of glass transition temperature, acid number, hydroxyl number and viscosity of the resin that characterize the quality of the product [3]. Commercial saturated polyester resins are manufactured predominantly from a combination of polycarboxylic compounds including isophthalic acid, terephthalic acid, adipic acid, trimellithic acid anhydride and the polyalcohols ethylene glycol, neopentylglycol, trimethylolpropane and glycerol. The production process required to achieve high molecular weight carboxyl-functional saturated polyester resins is a two stage esterification, in which the first stage involves the preparation of a precondensate by reacting the acids with excess of diols, and a second stage by reacting the remaining diols with additional acids.

For polyester production, chemometric modelling has been used to correlate analytical properties such as acid number [4-8] and hydroxyl number [4, 6-8] with offline NIR spectra. Offline analysis satisfies the needs for quality control tests, but it is time and labour intensive. Hence, it is not efficient enough to implement feedback control in an industrial production process. For continuous process monitoring, in situ NIR methods could offer a better approach. However, in situ NIR spectra are greatly affected by the physical and chemical variations found in large-scale reaction systems [9]. For instance, the variation of process variables such as temperature [10], the presence of two-phase interfaces between liquid and solids [11, 12],

88 immiscible liquids and gas bubbles [13], the change in optical properties of the material during
89 reaction [8], as well as changes in the NIR instrumentation (e.g. temporal variation of
90 illumination, changes in light transmission due to fiber optics related issues [13]), need to be
91 addressed on a case-by-case basis. As a result, transferring the advantages of offline NIR
92 spectroscopy to real time process monitoring remains a challenge for the polyester industry and
93 for similar applications.
94 To generate process understanding through online NIR monitoring, chemometric models
95 including partial least squares (PLS) regression are typically used to correlate the key analytical
96 properties with the online measured spectra [8]. Likewise, end-point detection models based
97 on principal component analysis (PCA) for multivariate statistical process control (MSPC)
98 have been used to control the process evolution through sole spectral variations [14-16].
99 Requirements that must be followed in building these models include the need for calibration
100 data sets to be representative of future process data [17], and that pre-processing steps need to
101 be applied to prevent the negative effects from process disturbances in the quality of the
102 spectral signal [18, 19]. When these issues are not addressed, accuracy and robustness of the
103 chemometric models is compromised [20]. Any action directed to improve the quality of the
104 spectra acquired, minimising the effect of disturbing factors on the signal and the models, is
105 highly beneficial [21].
106 In this context, the quality of the online NIR spectra depends on two main factors: the
107 interactions of the process disturbances with the process interface, and the method or
108 acquisition strategy implemented by the spectrometer selected for the application [22].
109 Additionally, conventional spectrometers are often installed in safe areas distant from the
110 process vessels, limited by their size, high cost and mechanical stability to obtain the demanded
111 performance. These requirements impact in both the instrumentation installation cost and the
112 quality of the online NIR signal used.

A recent alternative to the use of conventional spectrometers are spectral sensors using miniaturised and low cost MEMS-FPI chips (micro-electro mechanical system – Fabry-Pérot interferometer) developed for NIR wavelengths. MEMS-FPI are miniaturised tuneable optical filters that limit the pass of light in a narrow frequency range by using a set of two facing reflectors separated by an adjustable gap modified with a change in voltage [23]. These micro devices allow the scanning of specific regions of the spectra relevant to the process application, without incorporating moving parts such as those found in conventional FTIR spectrometers; and without diffraction gratings such as those found in dispersive spectrometers. These devices have additional advantages over conventional systems [24]: the size of the MEMS-FPI chip and the detector are considerably reduced, the system is position and vibration insensitive, and the spectral resolution does not suffer from tilting effects. Also, the device is very stable over time since the fabrication from a single wafer, without any additional assembly steps, creates a single solid structure with no wearing parts. Finally, thermal stabilization of the detector is straightforward because only a single-point detector is used, compared to conventional technologies that normally require linear array detectors [25]. MEMS-FPI sensors have been used for mid infrared (MIR) [26] and lately for NIR [27] applications, with a wide industrial application potential [28-30], although they still require further validation under a variety of laboratory and industrial conditions to understand their limitations and develop their potential further.

This paper investigates the use of a novel MEMS-FPI spectral sensor to monitor the high temperature production of saturated polyester resins. The performance of the novel NIR device was evaluated under the complex multiphase reaction conditions by using the online spectral information combined with PLS regression models to predict acid number and viscosity, and to identify the process end-point by using MSPC tools. The potential benefits to the process industry in terms of miniaturisation and low cost offered by these sensors were also explored.

2. Materials and methods

2.1 Reaction system

Twelve experimental batches of the saturated polyester resin were synthesised following a commercial process description at Megara Resins industrial facility in Greece. For the reaction, industrial grade terephthalic acid, isophthalic acid and adipic acid were the dicarboxylic acids used; ethylene glycol, diethylene glycol, neopentyl glycol, trimethylolpropane and glycerol were the polyols used. Butylstannoic acid was used as the esterification catalyst. The reagent ratios are kept undisclosed for confidentiality.

A 2 litre round flask with external heating and temperature control was used as the reaction vessel, keeping a continuous stirring rate of 200 rev per min. In order to prevent the discoloration due to the oxidation reaction, the reactor was continuously purged with nitrogen. In the first step, the reactant mixture was prepared by adding the fraction rich in diols into the vessel at approximately 80 °C. Once the diols were melted, the fraction rich in acids was added to the vessel under constant agitation. The temperature was then ramped up to 180 °C, where it was held for a 3 hour period, then increasing 20 °C every 3 hours up to reaching 240 °C, where the first reaction stage proceeds.

A hydroxyl-terminated polyester was formed by reacting the dibasic acids, polyols and optional branching agents like trimethylolpropane at a temperature in the range of 160 to 240 °C in the presence of esterification catalyst and colour stabilizer to form a hydroxyl-terminated prepolymer. At this stage, the water of esterification was collected. When the acid number of the resin fell below the value determined by the specifications, the first stage of the reaction was completed, providing a hydroxyl terminal polyester. In the second stage, the hydroxyl groups were end-capped with carboxylic acids or their anhydrides to form a carboxylated polyester. The amount of end-capping agent used was determined by the hydroxyl number of the polyester. The end-capping agent was added to the prepolymer and the esterification was

continued until the desired acid number was obtained. Vacuum was applied towards the end of the reaction in order to eliminate volatile products and thus shift the equilibrium towards the formation of the polymer. Finally, after a period determined by the analytical indicators, the temperature was lowered to 200 °C to add product enhancing additives and finish the production process.

2.2 Key analytical indicators

The analytical indicators selected to follow the progress of the reaction were acid number (AN) and viscosity (μ). Acid number was measured by manual acid-base titration following the ASTM (American Society for Testing and Materials) method D 1613-03 and it was reported as milligrams of potassium hydroxide (KOH) per gram of sample. Viscosity (high shear viscosity) was measured using a cone/plate viscometer model CAP 2000 from Brookfield (USA), operating at 200 °C following the procedure described in the ASTM method D-4287-00.

The targeted ranges for the first reaction stage were AN 8-12 (mg KOH g^{-1}) and μ 10-14 (P or g cm^{-1} s^{-1}); and for the second reaction stage AN 45-63 (mg KOH g^{-1}) and μ 25-45 P. In case the measurements were out of specifications during any of the stages, additional reactants were added to reach the desired conditions. During the analytical sampling, online NIR spectra were collected simultaneously from the reaction vessel.

2.3 MEMS-FPI NIR sensor and data acquisition

A novel spectral sensor model N-Series 1.7 by Spectral Engines (Finland) was used for the acquisition of the NIR spectra from 1350 nm to 1650 nm. A diagram of the sensor is shown in Fig. 1. The sensor has a single element extended InGaAs detector, with a tuneable MEMS-FPI filter acting as the spectral element. The sensor had an integrated light source model LS-PRO equipped with a miniature tungsten vacuum lamp as the illumination source. Additional details about the scanning mechanism used by the sensor can be found in the appendix section.

188 The spectral sensor was connected to a stainless steel NIR immersion probe (transmission
189 mode, 5 mm optical pathlength) model Excalibur 20 by Hellma Analytics (Germany). The
190 probe has two 2 m fibre optic cables, connecting one end to the light source and the other to
191 the spectral sensor. The probe was designed to operate from ambient temperature up to 260 °C,
192 and it was immersed with the transmission gap positioned towards the centre of the vessel
193 (facing the vessel agitator) during the entire reaction time, without observing solids depositing
194 into the probe for any of the batches performed.
195 For all experiments, the energy output for the lamp was set to 25% of the maximum level. This
196 value was selected for the specific polymerisation system investigated, since higher values
197 saturated the maximum input of the sensor and lower values were attenuated by the sample.
198 The sensor integration time was set to 0.1 ms and the wavelength step set to 1 nm (301 points
199 obtained from the operational sensor range).
200 The software used to operate and record NIR data from the spectral sensor was an in-house
201 application developed by the University of Leeds using LabVIEW 2015 (ChemiView V 3.4
202 [31]). Process temperature readings were acquired using a TC-08 temperature reader from Pico
203 Technologies (USA), using K-type immersion temperature probes from Omega (UK). For
204 batches 1 to 10, a single NIR spectrum was obtained every 5 s as the average of 50 sensor
205 readings (internal FPI scanning sequence implemented by the sensor, delivering 1 raw spectra
206 every 5 s). For batches 11 and 12, each NIR spectrum was obtained every 0.83 s from a single
207 FPI scanning sequence (minimum possible). The information for all batches is included in
208 Table 1, with batches labelled according to the sequence of acquisition.
209 **2.4 Process data treatment**
210 Multivariate calibration models using PLS regression to determine AN and μ parameters and
211 PCA-based MSPC models for end-point detection were created from the online NIR data. In
212 both cases, modelling and validation were carried out with in-house routines programmed in

Matlab R2017a (Mathworks, USA) and PLS_Toolbox 8.2.1 (Eigenvector Research, USA) running under Matlab.

For each batch, the influence of process disturbances in the quality of the NIR signal was considerable (discussed within results). In order to attenuate these effects, a pre-processing step was introduced. In this, 13 raw spectra (as delivered by the sensor) were averaged into a single spectrum, emulating the averaging that can be instrumentally obtained by increasing the number of FPI scans. This action reduced the number of spectra and the noise in the signal, at the expense of introducing a small delay time of 65 s per usable spectrum. Afterwards, the resulting averaged signal was transformed to absorbance. Since artifacts could not be completely removed, a moving average filter was applied to the absorbance spectra in the time dimension. Each spectrum was replaced by the average of itself and the N = 30 previous spectra, where N was chosen as a compromise between small prediction delay and good quality. This means 30 absorbance spectra are required to build-up the moving average before the data can be used for monitoring purposes, which occurs at the beginning of the process at a stage in which predictions are not required (latent phase, discussed in results). Finally, a 1st order Savitzky-Golay derivative [32] followed by column mean-centring was applied to correct baseline variations before submitting the resulting dataset to the PLS algorithm or to the end-point detection model. Under these conditions, the models deliver 1 prediction every 65 s.

(a) PLS regression models: The polymerisation process has two very distinct reaction stages, the first stage to form the hydroxyl-terminated prepolymer, and the second reaction stage to form the final carboxilated polyester. Therefore it was not possible to develop a single PLS for each property (AN and μ) that could provide predictions accurate enough for the entire process. The solution was to develop a PLS model for each property and for each stage, resulting in four multivariate calibration models relating the calibration spectra to AN and μ using PLS regression [33]. The averaged absorbance spectra corresponding to the times when samples

were collected during the reaction (known acid number and viscosity) were placed as the rows of data matrix **X** (samples × wavelengths). The reference values of acid number and viscosity made up column vectors $\mathbf{y}_{av}$ (samples × 1) and $\mathbf{y}_{vi}$ (samples × 1), respectively, and a separate model was completed to relate each of these properties to the NIR information. Because there are two clear different stages in the process, **X**, y_{av} and y_{vi} were split in two sets, one for the first stage of the reaction ($\mathbf{X}_1$, $\mathbf{y}_{av,1}$ and $\mathbf{y}_{vi,1}$), and another for the second stage of the reaction ($\mathbf{X}_2$, $\mathbf{y}_{av,2}$ and $\mathbf{y}_{vi,2}$). Pre-processed NIR spectra from batches 1 to 5 were used to generate the training set for the PLS models, with 7 additional batches used as external validation set.

(b) MSPC models: To build MSPC models, a data set formed by NIR spectra collected at the end of each stage from normal operating condition (NOC) batches were used. All the end-point spectra were organized in a data matrix $\mathbf{X}_{NOC}$ (number of end-point NIR spectra × wavelengths). A PCA model was built with these data to set the statistical boundaries of the experimental domain (space) of end-point NIR spectra [34, 35]:

$$\mathbf{X}_{NOC} = \mathbf{T}_{NOC}\mathbf{P}_{NOC}^{T} + \mathbf{E}_{NOC}$$

where $\mathbf{T}_{NOC}$ is the scores matrix of all end-point spectra (spanning the valid experimental domain for on-specification measurements in the space of principal components) and $\mathbf{P}_{NOC}^{T}$ is the loadings matrix (which is the link between scores and original NIR spectra). $\mathbf{E}_{NOC}$ describes the residual variation unexplained by the PCA model. The number of components used in the PCA model was established by cross-validation [36]. From the PCA model, a Q-statistic control chart Q_{stat} was built, the boundary of which was based on the residual part of the process variation not explained by the PCA model. The control limit for the Q_{stat} chart, Q_{lim}, was set according to the Jackson and Mudholkar equation [37]. For any new (pre-processed) spectrum acquired in an online monitored batch, $\mathbf{x}_{i,new}$, the PCA model obtained above was used as follows (additional details can be found in appendix section):

$$\mathbf{t}_{i,new} = \mathbf{x}_{i,new}\mathbf{P}_{NOC}$$

For this study, data from on-specification batches 2 to 5 were used to extract NIR data to build an initial end-point detection model. Subsequently, data from batches 2 to 9 were used to build an updated version of the same model. The remaining batches out of their modelling sets were used for cross-validation. The pre-processed NIR spectra used were collected during the last 15 minutes before the end of each reaction stage for each batch. Two matrices with 60 spectra (4 batches x 15 spectra) were generated with the selected end-point NIR spectra to build two separate end-point MSPC models for stages 1 and 2 of the process. Spectral pre-processing was performed as explained above.

3. Results and discussion

3.1 Saturated polyester resin production process and online NIR sampling

The production of saturated polyester resins progressed as a multiphase reaction, in which gas bubbles and suspension solids considerably affected the spectral measurements during all the process stages. Fig. 2 (top) shows images of the different reactions periods relating the presence of bubbles, solid particles, while Fig. 2 (middle and bottom) presents related fluctuations in temperature and the NIR signal by these process disturbances in the time domain.

For instance, at the beginning of the process, the carboxylic acids were solids in suspension forming the liquid polymer as the reaction progresses. The solids totally attenuated the NIR signal over the initial 10-12 hours of the process (also known as latent phase; Fig. 2, a), which gradually changed as the carboxylic acids reacted and the solution became transparent to NIR light at the beginning of the first reaction stage (Fig. 2, from a to b), clearing further towards the end of this (Fig. 2, c). During the latent phase, light absorption and scattering produced by the particles were the predominant effect. This phenomenon occurred again when the chemicals for the second reaction stage were added (a large fraction of carboxylic acids in solid form), and also when performing small corrections (adding small quantities of the same solids) required to drive the analytical properties towards the desired values (Fig. 2, d).

Simultaneously, as the reaction progressed, gas bubbles were generated due to the formation of water and low boiling point products resulting from the transesterification reactions, and also due to the nitrogen stream passing through the reaction mixture. These bubbles tended to remain in the system for extended periods of time due to the high viscosity of the mixture, which dissipated slowly when reaching the surface of the vessel or forced to leave when a vacuum was applied to the system. The last action also contributed to drive the key analytical properties towards the desired values. Bubbles scattered the NIR light, but still allowed a usable signal to reach the detector. Bubbles appeared at the intermediate phases of each reaction stage,

296 when the solids had completely reacted. Towards the end of each reaction stage, bubbles also
297 gradually disappeared, with the sample becoming fully transparent (Fig. 2, e).
298 Finally, the temperature of the reactor also fluctuated around the set point of the heating control
299 as shown by the temperature readings and mirrored by the NIR spectra, particularly noticeable
300 during the latent phase (Fig. 2, blue line). Fluctuations were due to the limitations of the heating
301 element control. When none of these phenomena disturbed NIR acquisition, the signal had a
302 stable amplitude and was very repeatable between scans, especially at the end of the reaction
303 process (Fig. 2, f).
304 Compared to previous reports using offline NIR spectra to correlate key analytical properties
305 [6], the fluctuations produced by process disturbances in the NIR spectra were the main
306 obstacle to perform online monitoring. The attenuation effect produced by solid particles was
307 the main restricting factor that limited the time window to obtain useful NIR measurements in
308 transmission mode. On average, the complete reaction process takes approximately 25 hours
309 per batch, from which the first 12 to 14 hours corresponded to the latent phase (non-
310 transparent), with periods of approximately 5 hours for each reaction stage (transparent). Under
311 these conditions, the time frame for measuring useful NIR spectra that could be correlated to
312 the key analytical properties was 3-6 hours for each stage. Fig. 2 illustrates the NIR monitoring
313 window observed for batch number 5.
314 Fig. 3 shows groups of five consecutive NIR scans (raw intensity spectra, thin blue lines) and
315 their corresponding average (red dashed lines), obtained for specific periods of the first (i) and
316 second (ii) reaction stages during the NIR monitoring window. These groups correspond to
317 similar time periods for the specific process conditions shown in Fig. 2. As observed from Fig.
318 3, the intensity of the signal tends to increase as the reaction progress, with the exception of
319 the transition period between stages one and two, when a large fraction of solids was added
320 causing the signal to drop. Regarding the active NIR groups for the polyester system relative

to the spectral range of the NIR sensor used, the wavelength range 1400 – 1500 nm relating to first overtone of -OH vibration was the most important for prediction. It also allowed differentiating clearly between reaction stage 1 and stage 2 of the process. Although wavelengths longer than 1500 nm are less important for prediction, they allowed a better outlier detection and, therefore, the full wavelength range covered by the NIR spectral sensor was found useful for modelling purposes (an absorbance plot for the same spectra and time periods shown in Fig. 3 is available in Appendix).

3.2 Prediction of key analytical properties using PLS and MSPC models

For the 12 batches performed, the analytical indicators measured at the end of each stage and the final process outcome are listed in Table 1. Two out of twelve batches ended up out of specification in relation to the commercial product, after a reasonable number of attempts to correct the direction of the process towards the desired analytical control parameters. The time difference observed between batches was due to the number of chemical adjustments carried out for each case. After each chemical correction, it was necessary to wait for thermal stabilization of the system and the reaction of the solids in suspension before obtaining the next analytical measurement.

Fig. 4 compares the acid number determined offline (circles) and the continuous prediction generated from the online NIR spectra after applying the PLS models for six batches (batches 3 to 5 used for calibration, and batches 7 to 9 used for validation were included in this figure. Similar plots for all twelve batches can be found in Appendix). The analytical measurements and the predictions shown in these figures were obtained during the NIR monitoring window, in which the time gap between reaction stages corresponded to the addition of the second stage chemicals (solids).

Continuous predictions obtained from the PLS models against the offline viscosity measurements are shown in Fig. 5, illustrating the same batches used for Fig. 4. For both

346 process stages, viscosity values always increase due to the increasing length of the polymer
347 branches formed and the PLS model predictions followed this trend.
348 For both acid number and viscosity predictions, sharp variations between consecutive spectra
349 due to bubbles and solids in suspension were the most important data issue to be solved when
350 building and implementing PLS models. These variations affected the transmission of light
351 both in the wavelength dimension and in the time dimension randomly e.g. one spectrum may
352 suffer artifacts at certain wavelengths, while the next was affected at different wavelengths (as
353 shown in Fig. 3). Normally, the referential analytical properties vary slowly during the reaction,
354 except when adding chemical corrections to the system or when changing operational
355 parameters such as the flow of inert gas. Under normal conditions, it is expected that the model
356 predictions should also evolve slowly, although in this case process interferences still created
357 fluctuations that could not be completely attenuated. Spectrum averaging compensated these
358 undesired effects to a large extent, but could not completely remove them. The spectral moving
359 average over time improved the stability of the predictions, and the remaining fluctuations were
360 considered to be acceptable, taking into account the complexity of the data, and followed the
361 evolution of the process satisfactorily.
362 Regarding to the accuracy of the predictions obtained, Fig. 6 compares the acid number and
363 viscosity measured for the 12 batches against the predictions obtained from the PLS models.
364 From these figures, it is evident that both key parameters differed considerably for the second
365 reaction stage relative to those predicted for the first stage. Although the process fluctuations
366 observed in both cases were very similar, changes in the first reaction stage were slower and
367 observed at the end of longer time period (latent phase + first reaction stage). Conversely, for
368 the second reaction stage, changes were more vigorous and produced in a shorter time interval,
369 which led to slight increases to the variations on the NIR spectra and resulting predictions.

370 Results generally indicated that acid number predictions were more precise for the first stage
371 than those obtained for the second stage. This difference can be explained by the chemistry of
372 the system, which has smaller changes during the first stage, as it reacts under an excess of
373 diols, with acid number ranging from 5 to 20 mg KOH g^{-1}. For the second reaction stage, the
374 end groups contributing to the acid number were targeted, with a variation fluctuating between
375 50 to 70 mg KOH g^{-1}, almost an order of magnitude higher compared to the first stage range.
376 Finally, it is noted that viscosity predictions were more precise and accurate relative to those
377 obtained for the acid number. This difference may simply be due to the higher repeatability of
378 the analytical measurements obtained using the cone viscometer, compared to reference acid
379 number obtained by manual titration that had greater higher variability.
380 Models for acid number and viscosity were developed with the data obtained from batches 1
381 to 5 (from February 2017), and predictions for batches 6 to 12 considered new data (collected
382 in September 2017). As a consequence, there was some increase in prediction variability for
383 batches 6 to 12. Some of the slight reduction in predictive performance may have been due to
384 some introduced systematic bias, because the system had to be reinstalled in Megara after a six
385 month period. Even though the optical components e.g. fibre optic cables and sensors were the
386 same, the system setup was not absolutely be identical e.g. fibre bending radius and ambient
387 temperature was not exactly the same. However, even accounting these differences, the model
388 prediction was within an acceptable range e.g. within the intrinsic error of the wet chemistry
389 analysis, and highlighted the real potential to use the NIR system for process monitoring.
390 Additionally, information from the PCA models obtained directly from the sole NIR spectra
391 (without using calibration samples) provided another perspective to evaluate the use of the
392 MEMS-FPI sensors. Fig. 7 shows the end-point detection MSPC model predictions obtained
393 for all the batches during the NIR monitoring window, using an initial model created with
394 batches 2 to 5 (black symbols). For a better visualization of the control chart and the related

limit, reduced Q-statistics (Q_{red}), expressed as, $Q_{red} = Q_{stat}/Q_{lim}$, were used. In this way, the limit in all Q_{red} charts is equal to 1. An initial qualitative analysis from the profiles suggests a clear decreasing pattern of the Q_{stat} values as the process progresses towards completion. Although, the overall final end-point values obtained could be more precise, given the complete experimental set, initial model performance was acceptable, considering the small number of available batches used to build the PCA model.

However, in order to improve the definition of the process end-point, the PCA-based MSPC models were updated to include a larger number of batches (2 to 9). Batches 10 to 12 were not included in the updated model and used for external model validation. Predictions using the updated model are also shown in Fig. 7 (red dots). Analysing the validation batch 10, we can observe that its second stage did not reach the end-point control limit, which agrees with experimental observation reported in Table 1, where this batch was considered as out of product specification. Although on specification batches 11 and 12 did not cross the end-point control limit for long time, they showed trend towards it, which indicates that these batches could be accepted according to these observations. The results suggest that a larger number of batches will improve the repeatability and robustness of the control models implemented, and that the sole online NIR information obtained from the sensor was sensitive enough to detect the process end-point.

The effect of the process disturbances was also observed for the PCA-based models, although its influence in the identification of the end-point reached for each stage was limited. This is explained by the quality of the selected NIR spectra used to build the end-point detection model, which correspond to the last 15 minutes of each stage. This particular time interval of the process had two key distinctive differences; firstly, the NIR spectra collected have a higher optical transmittance since the presence of bubbles and solids present was minimum at the end of each stage (Fig. 2, c and f). Secondly, there was a clear difference in the shape of the

absorbance spectra at the ending period compared to the initial reaction interval, which produced more intense NIR profiles with stronger peak association (Fig. 3 illustrated this).

The use of a large number of averages to minimise the influence of process disturbances in the NIR spectra had a small impact on the response time of the MSPC model predictions. However, it was not great enough to hide the fluctuations produced by adding corrective chemicals to the reaction vessel (emphasized in Fig. 7 for batches 1 and 10, although this action was performed for most of the batches) to drive the key analytical parameters to their control values. Since the anticipated outcome for this model was a single parameter to identify the process end-point, the implementation was simpler than predicting the analytical properties over short time intervals and required only NIR spectra for generating the training set, without any additional experimental calibration.

Finally, the results obtained from the PLS prediction of viscosity and acid number can be used together with the MSPC control chart to provide additional supporting information to the end-user. Although using the PLS models as an alternative to the traditional offline analytical analysis still need to be further demonstrated, the results obtained show clearly the NIR sensor performance, even when challenged by severe process fluctuations encountered in the pilot scale process. Under these conditions, predicted viscosity and acid number were within the acceptable limits required for monitoring the synthesis of saturated polyester resins.

In addition, the miniaturised size was a distinctive characteristic of the MEMS-FPI sensor, which enabled its installation attached to the reaction vessel, minimising the use of fibre optics cables for transmitting the NIR light. Instead, a standard electrical signal was transmitted from the sensor to the computer, reducing the installation and maintenance costs considerably. Another factor to consider was the stability observed for the MEMS-FPI sensor during the experimental trials, allowing to maintain the calibration for the PLS-based and end-point models. In this study, the whole system was dismounted and reassembled between the two

445 experimental campaigns and, although updated models offered better results, predictions based
446 on the models initially built were still acceptable for the 7 new batches.
447 Besides, access to affordable process monitoring and control technologies for small and
448 medium enterprises (SMEs) has been identified as a contributing factor to improve process
449 sustainability [38]. For the synthesis of polyester resins (or similar challenging reactions), real-
450 time access to the key process indicators can minimise the number of manual sampling points
451 collected from the high temperature reaction vessels, helping to reduce the risks associated to
452 a minimum. Also, this low-cost information can help to improve batch-to-batch consistency
453 e.g. observing the development of detrimental disturbances in real-time, and implementing
454 control actions faster than using the off-line data (time delayed); avoiding the loss of materials
455 and equipment due to batch failure. Finally, access to online monitoring tools can help SMEs
456 to implement more advanced process optimisation strategies, saving cycle time by reducing the
457 number of off-line controls, and bringing further reductions in material consumption and
458 energy savings.

459 The use of this new generation of MEMS-FPI NIR sensors appears to be a suitable alternative
460 to traditional spectroscopy systems, and particularly adapted to harsh industrial environments
461 such as the production of saturated polyester resins.

4. Conclusion

A new MEMS-FPI NIR sensing technology combined with suitable chemometric data processing was used for effective monitoring of multi-phasic production of saturated polyester resins. This process presented several challenges, which are often encountered in similar industrial applications, including variations between spectra, due to the presence of bubbles and solids particles in suspension, and temperature fluctuations. These process disturbances affected the transmission of light both in the wavelength and in the time domains, and also limited the time window to observe the reaction in NIR transmission mode. These issues where addressed by extensive pre-processing and allowed satisfactory implementations of PLS and PCA-based end-point detection models. In addition, the stability of the optical system over a long time period, achieved by the single frame MEMS-FPI chip architecture and integrated light source, helped to generate a high quality and robust NIR signal. Hence, the combination of the notable optical properties of the sensor combined with chemometric tools to address process-related signal distortions, provided excellent results for monitoring of the key analytical properties (acid number and viscosity) as well as end-point control. This new generation of NIR sensors presented a number of advantages over traditional spectral systems, such as miniaturisation, low cost and stability, providing an affordable alternative to improve process performance, reduce costs and contribute to sustainability in the process industry.

Acknowledgements

This work was supported by the ProPAT Project (European Union Horizon 2020 research and innovation programme under grant agreement 637232). The authors thank Megara Resins for facilitating their facilities for this study.

References

[1] Saturated polyester resin market worth $4,436 million by 2019, Focus on Powder Coatings, 2015 (2015) 7.
[2] M.P. Stevens, Polymer chemistry : an introduction, 2nd ed., Oxford University Press, New York ; Oxford, 1990.
[3] B. Parkyn, Chemistry of polyester resins, Composites, 3 (1972) 29-33.
[4] E. Marengo, M. Bobba, E. Robotti, M. Lenti, Hydroxyl and acid number prediction in polyester resins by near infrared spectroscopy and artificial neural networks, Analytica Chimica Acta, 511 (2004) 313-322.
[5] S.R.K. Chalasani, S. Dewasthale, E. Hablot, X.K. Shi, D. Graiver, R. Narayan, A Spectroscopic Method for Hydroxyl Value Determination of Polyols, J Am Oil Chem Soc, 90 (2013) 1787-1793.
[6] M. Blanco, J. Cruz, M. Armengol, Control production of polyester resins by NIR spectroscopy, Microchemical Journal, 90 (2008) 118-123.
[7] M. Blanco, V. Villaescusa, Use of NIR spectroscopy in the production of modified industrial resins, Talanta, 71 (2007) 1333-1338.
[8] R.A. Heikka, K.T. Immonen, P.O. Minkkinen, E.Y.O. Paatero, T.O. Salmi, Determination of acid value, hydroxyl Value and water content in reactions between dicarboxylic acids and diols using near-infrared spectroscopy and non-linear partial least squares regression, Analytica Chimica Acta, 349 (1997) 287-294.
[9] N. Heigl, C.H. Petter, M. Rainer, M. Najam-ul-Haq, R.M. Vallant, R. Bakry, G.K. Bonn, C.W. Huck, Near Infrared Spectroscopy for Polymer Research, Quality Control and Reaction Monitoring, Journal of Near Infrared Spectroscopy, 15 (2017) 269-282.
[10] O.R. Ghita, D.C. Baker, K.E. Evans, An in-line near-infrared process control tool for monitoring the effects of speed, temperature, and polymer colour in injection moulding, Polymer Testing, 27 (2008) 459-469.
[11] M.M. Reis, P.H. Araujo, C. Sayer, R. Giudici, Spectroscopic on-line monitoring of reactions in dispersed medium: chemometric challenges, Anal Chim Acta, 595 (2007) 257-265.
[12] M.M. Reis, P.H.H. Araujo, C. Sayer, R. Giudici, In situ near-infrared spectroscopy for simultaneous monitoring of multiple process variables in emulsion copolymerization, Ind Eng Chem Res, 43 (2004) 7243-7250.
[13] Y.J. Wu, Y. Jin, Y.R. Li, D. Sun, X.S. Liu, Y. Chen, NIR spectroscopy as a process analytical technology (PAT) tool for on-line and real-time monitoring of an extraction process, Vibrational Spectroscopy, 58 (2012) 109-118.
[14] T.A. Catelani, J.R. Santos, R. Pascoa, L. Pezza, H.R. Pezza, J.A. Lopes, Real-time monitoring of a coffee roasting process with near infrared spectroscopy using multivariate statistical analysis: A feasibility study, Talanta, 179 (2018) 292-299.
[15] H. Huang, H. Qu, In-line monitoring of alcohol precipitation by near-infrared spectroscopy in conjunction with multivariate batch modeling, Anal Chim Acta, 707 (2011) 47-56.
[16] R.R. de Oliveira, C. Avila, R. Bourne, F. Muller, A. de Juan, Data fusion strategies to combine sensor and multivariate model outputs for multivariate statistical process control, Anal Bioanal Chem, 412 (2020) 2151-2163.
[17] D.S. Bu, B.Y. Wan, G. McGeorge, A discussion on the use of prediction uncertainty estimation of NIR data in partial least squares for quantitative pharmaceutical tablet assay methods, Chemometrics and Intelligent Laboratory Systems, 120 (2013) 84-91.

[18] Z. P. Chen, J. Morris, Pat: The Extraction of Maximum Information from Messy Spectral Data, IFAC Proceedings Volumes, 40 (2007) 7-12.
[19] A. Cherfi, G. Fevotte, C. Novat, Robust on-line measurement of conversion and molecular weight using NIR spectroscopy during solution polymerization, Journal of Applied Polymer Science, 85 (2002) 2510-2520.
[20] T. Chen, E. Martin, The impact of temperature variations on spectroscopic calibration modelling: a comparative study, Journal of Chemometrics, 21 (2007) 198-207.
[21] A.E. Cervera, N. Petersen, A.E. Lantz, A. Larsen, K.V. Gernaey, Application of near-infrared spectroscopy for monitoring and control of cell culture and fermentation, Biotechnol Prog, 25 (2009) 1561-1581.
[22] C. Pasquini, Near infrared spectroscopy: A mature analytical technique with new perspectives - A review, Anal Chim Acta, 1026 (2018) 8-36.
[23] O.S. Heavens, The Fabry-Perot-Interferometer - History, Theory, Practice and Applications - Vaughan,Jm, Nature, 341 (1989) 194-194.
[24] J. Antila, M. Tuohiniemi, A. Rissanen, U. Kantojärvi, M. Lahti, K. Viherkanto, M. Kaarre, J. Malinen, MEMS- and MOEMS-Based Near-Infrared Spectrometers, Encyclopedia of Analytical Chemistry2014, pp. 1–36.
[25] A. Rogalski, Progress in focal plane array technologies, Prog Quant Electron, 36 (2012) 342-473.
[26] M. Blomberg, A. Torkkeli, A. Lehto, C. Helenelund, M. Viitasalo, Electrically tuneable micromachined Fabry-Perot interferometer in gas analysis, Phys Scripta, T69 (1997) 119-121.
[27] A. Akujarvi, B. Guo, R. Mannila, A. Rissanen, MOEMS FPI sensors for NIR - MIR microspectrometer applications, Proc Spie, 9760 (2016).
[28] H. Vakili, H. Wickstrom, D. Desai, M. Preis, N. Sandler, Application of a handheld NIR spectrometer in prediction of drug content in inkjet printed orodispersible formulations containing prednisolone and levothyroxine, Int J Pharm, 524 (2017) 414-423.
[29] A. Rissanen, B. Guo, H. Saari, A. Nasila, R. Mannila, A. Akujarvi, H. Ojanen, VTT's Fabry-Perot interferometer technologies for hyperspectral imaging and mobile sensing applications, Moems and Miniaturized Systems Xvi, 10116 (2017).
[30] C.R. Avila, J. Ferre, R.R. de Oliveira, A. de Juan, W.E. Sinclair, F.M. Mahdi, A. Hassanpour, T.N. Hunter, R.A. Bourne, F.L. Muller, Process Monitoring of Moisture Content and Mass Transfer Rate in a Fluidised Bed with a Low Cost Inline MEMS NIR Sensor, Pharm Res, 37 (2020) 84.
[31] C. Avila, ChemiView, 2015.
[32] P.A. Gorry, General Least-Squares Smoothing and Differentiation by the Convolution (Savitzky-Golay) Method, Analytical Chemistry, 62 (1990) 570-573.
[33] H. Martens, T. Naes, Multivariate calibration, Wiley, Chichester, 1989.
[34] T. Kourti, Application of latent variable methods to process control and multivariate statistical process control in industry, Int J Adapt Control, 19 (2005) 213-246.
[35] J.F. Macgregor, T. Kourti, Statistical Process-Control of Multivariate Processes, Control Eng Pract, 3 (1995) 403-414.
[36] S. Wold, Cross-Validatory Estimation of Number of Components in Factor and Principal Components Models, Technometrics, 20 (1978) 397-405.
[37] J.E. Jackson, G.S. Mudholkar, Control Procedures for Residuals Associated with Principal Component Analysis, Technometrics, 21 (1979) 341-349.
[38] H.A. Kishawy, H. Hegab, E. Saad, Design for Sustainable Manufacturing: Approach, Implementation, and Assessment, Sustainability, 10 (2018).

Table 1

Summary of analytical parameters measured, total reaction time and NIR spectra acquired

Batch	AN[a,c]	μ[a,d]	AN[b,c]	μ[b,d]	Final process outcome	Reaction time	NIR scans per single spectrum	Number of spectra
1[e]	8.4	7.0	-	-	Out of specification	21 h, 40 min	50 averaged in 5s	16427
2	6.0	16.0	49.9	36.4	Within specification	21 h, 10 min	50 averaged in 5s	16753
3	8.4	13.6	48.0	50.3	Within specification	26 h, 25 min	50 averaged in 5s	20052
4	7.9	14.5	55.6	36.7	Within specification	21 h, 25 min	50 averaged in 5s	16456
5	7,8	14,1	54.0	38,4	Within specification	22 h, 30 min	50 averaged in 5s	17230
6	8.4	9.6	51.0	29.9	Within specification	22 h, 20 min	50 averaged in 5s	16199
7	8.9	9.5	54.0	42.5	Within specification	22 h, 55 min	50 averaged in 5s	16621
8	9.5	12.3	54.0	39.1	Within specification	22 h, 5 min	50 averaged in 5s	15940
9	9.0	12.1	53.3	41.0	Within specification	24 h, 50 min	50 averaged in 5s	17970
10[f]	8.7	10.1	56.0	53.7	Out of specification	24 h, 15 min	50 averaged in 5s	17149
11	8.3	10.3	55.0	31.7	Within specification	24 h, 45 min	1 scan in 0.83s	104987
12	7.6	10.8	51.0	36.2	Within specification	21 h, 05 min	1 scan in 0.83s	92204

[a] At the end of the first reaction stage; [b] at the end of the second reaction stage; [c] AN in mg KOH g^{-1}; [d] μ in Poise; [e] batch 1 ended out of specification after first reaction stage; [f] batch 10 ended out of specification after the second reaction stage.

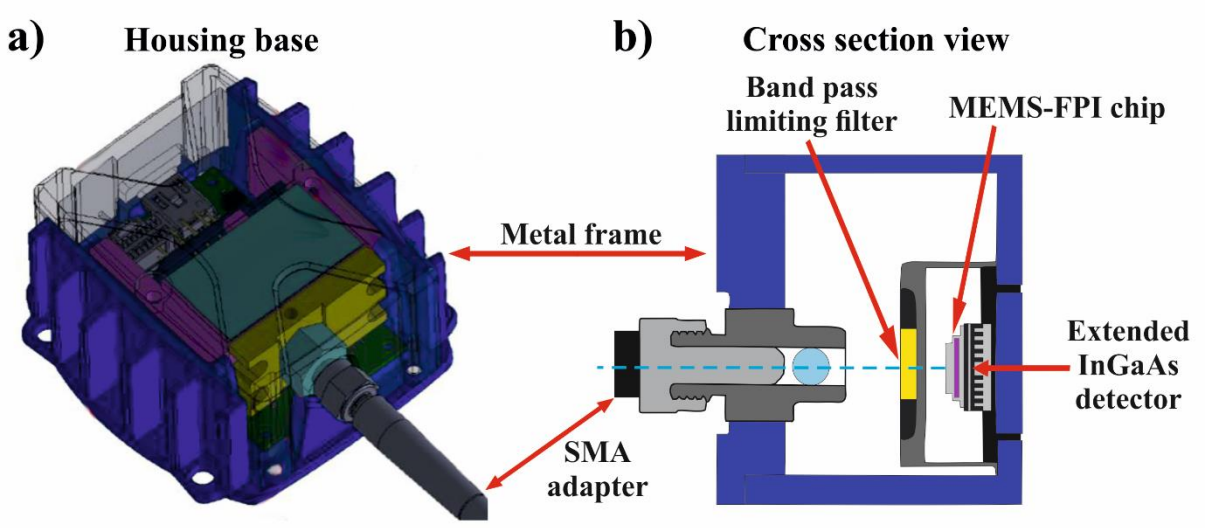

Fig. 1. Diagram of the NIR spectral sensor base (a) with the MEMS-FPI tuneable filter (b). The assembled sensor weight 125 grams, with the metal chassis measuring 58 mm length by 57 mm width by 27 mm high.

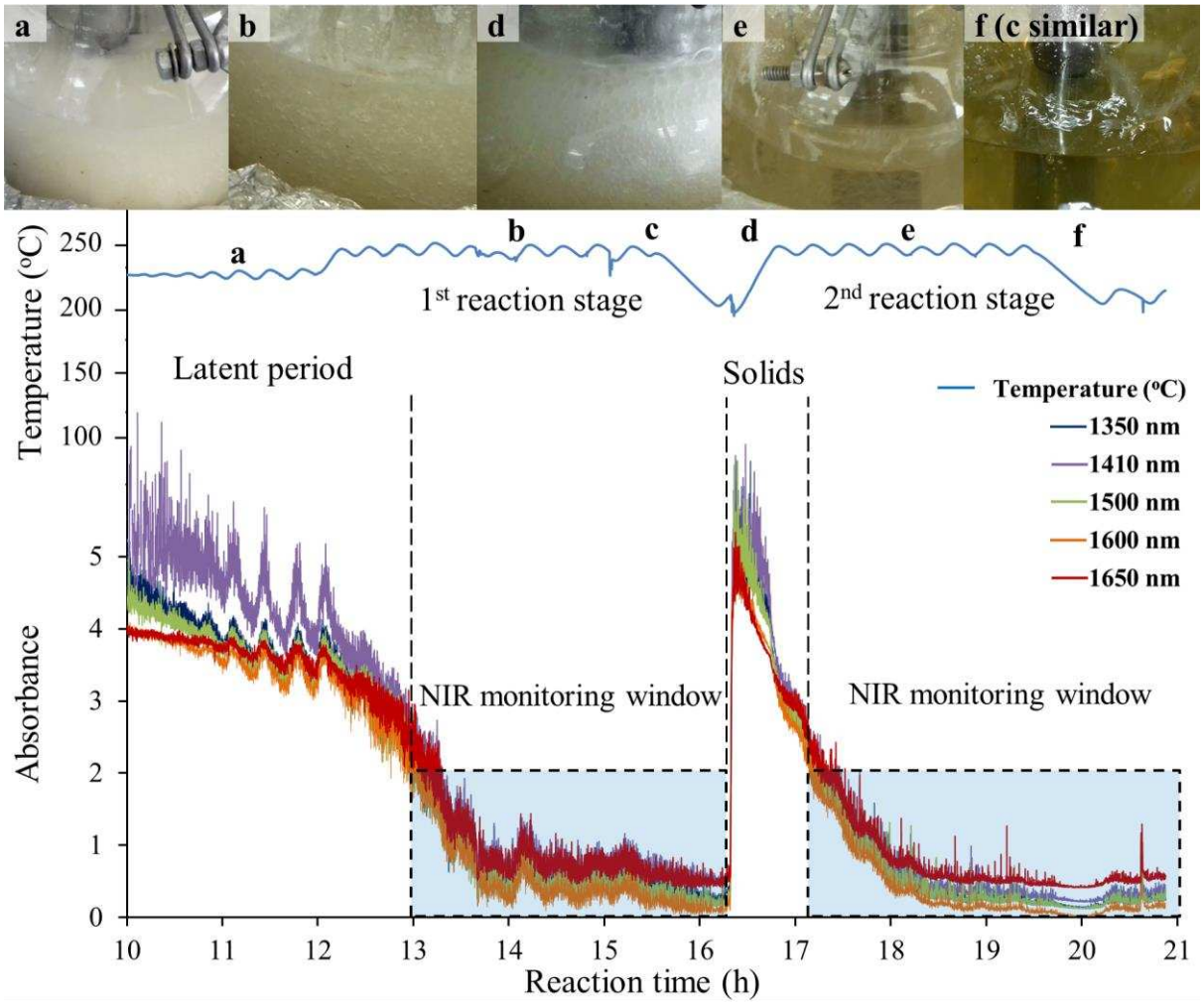

Fig. 2. Images showing typical process conditions (top): a) bubbles and solids in suspension during the latent phase; b) bubbles in suspension in the middle of first stage; c) homogeneous solution at the end of the first stage; d) bubbles and solids in suspension after adding second stage chemicals; e) bubbles in suspension in the middle of second stage; f) final product. The influence of temperature fluctuations (middle, blue line) mirrored by the absorbance NIR spectra for 5 selected wavelengths (bottom; for batch 5, similar to all batches) as a function of time, for the final 11 hours of the process.

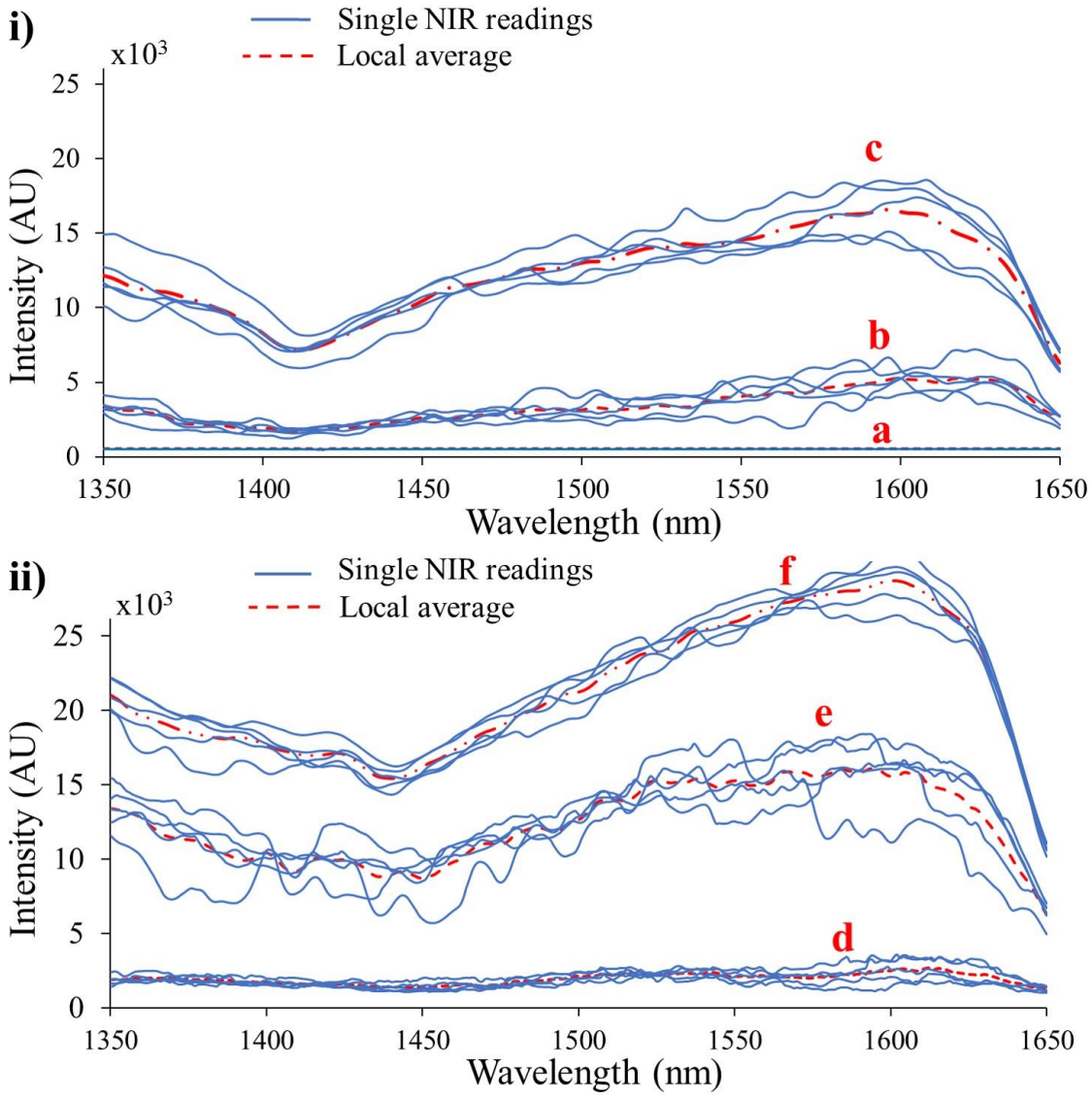

Fig. 3. Example NIR spectra shown for six different process periods, displaying the disturbances generated by bubbles and solids particles in suspension. i) First reaction stage: a) bubbles and solids in suspension during the latent phase; b) bubbles in suspension in the middle of first stage; c) homogeneous solution at the end of the first stage. ii) Second reaction stage: d) bubbles and solids in suspension after adding second stage chemicals; e) bubbles in suspension in the middle of second stage; f) final product. Data from batch number 5, and similar to all other batches. Groups of five consecutive raw spectra (thin blue lines), and red dashed lines corresponding to the average spectrum obtained for each group. Absorbance plot for the same spectra is available in Appendix.

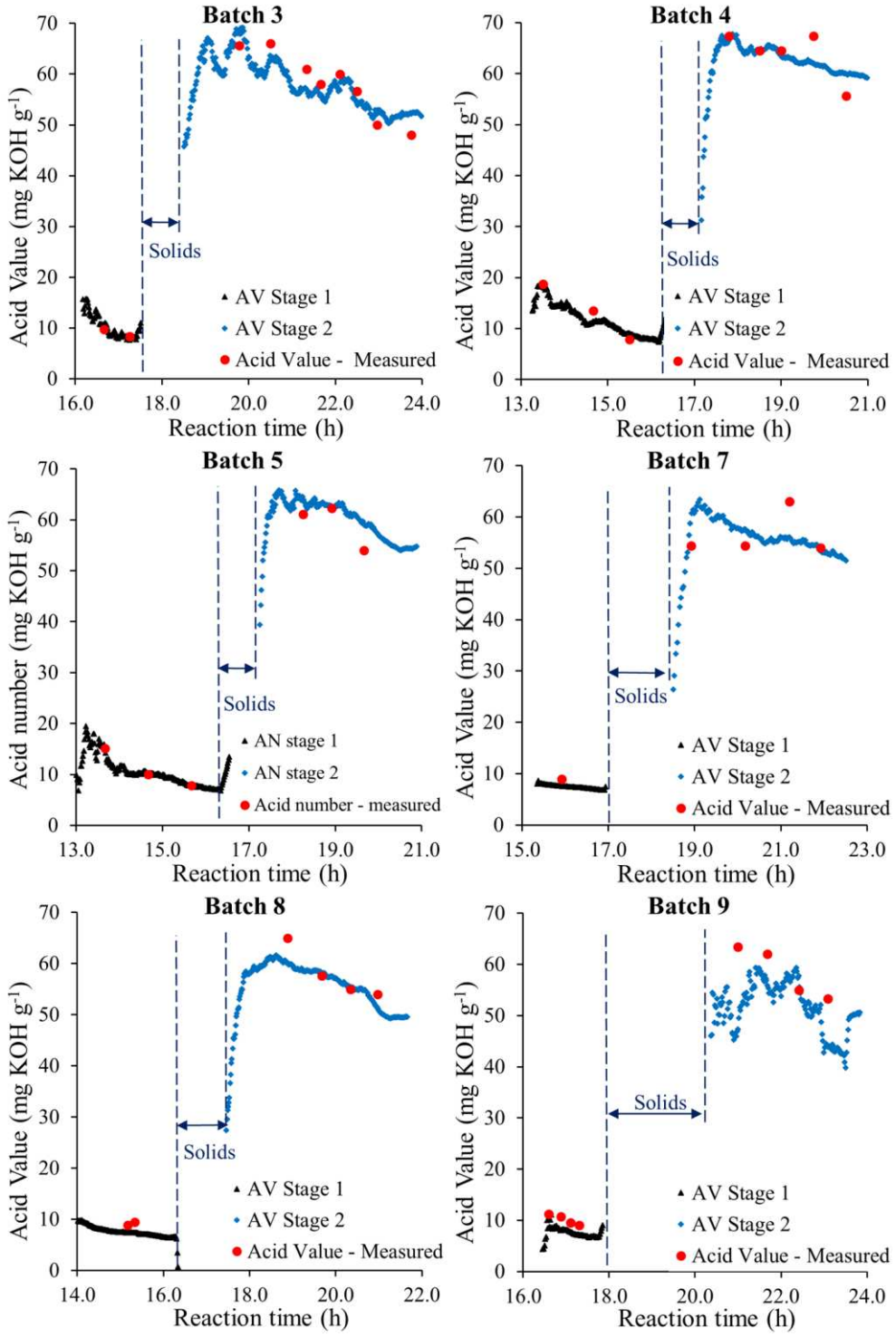

Fig. 4. Experimental acid number obtained (red dots) compared to continuous PLS model predictions based on NIR measurements, for the first and second reaction stages. Batches 3, 4 and 5 used for model making; batches 7, 8 and 9 used as external validation.

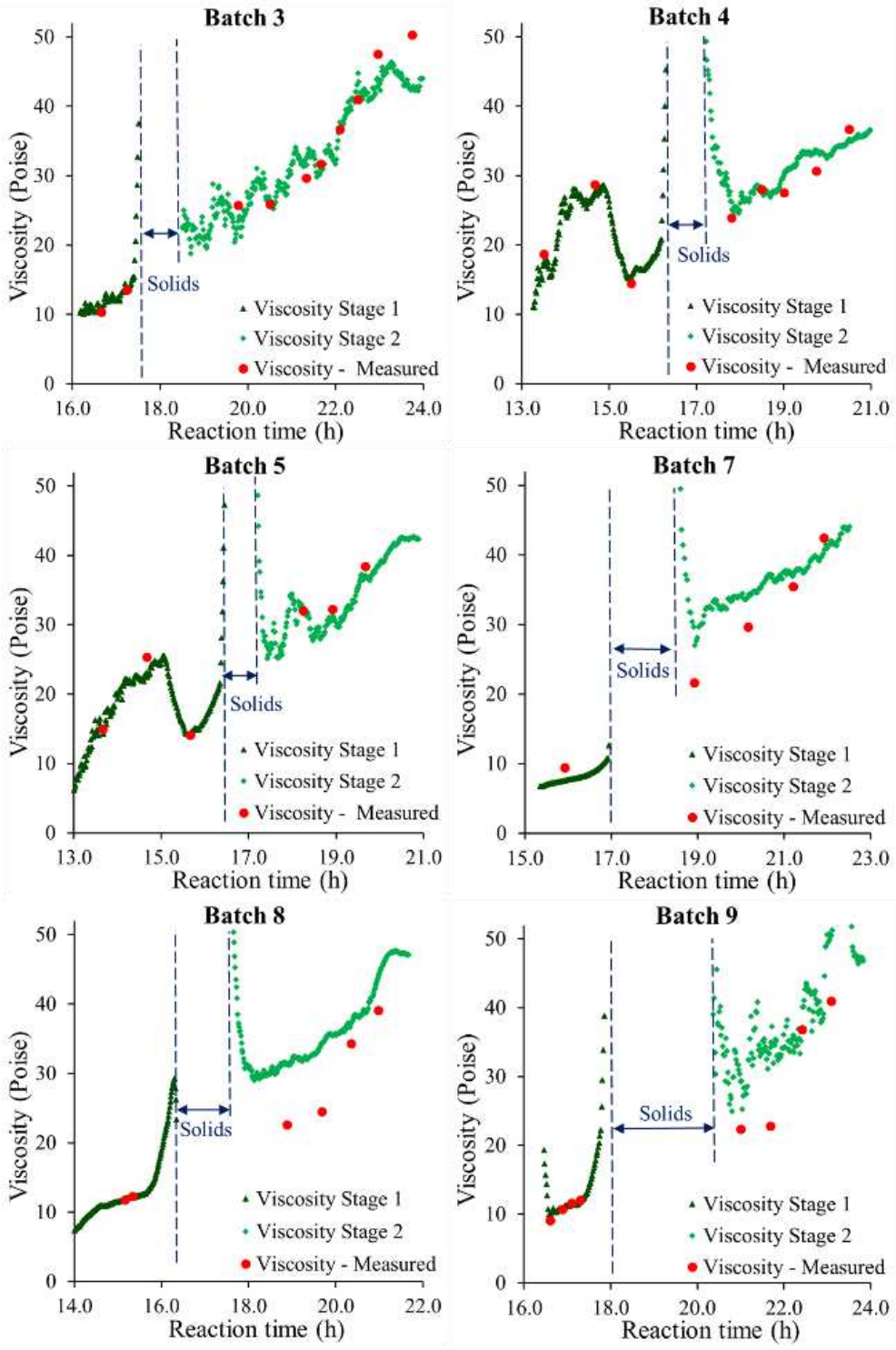

Fig. 5. Experimental viscosity values obtained (red dots) compared to continuous PLS model predictions based on NIR measurements, for the first and second reaction stages. Batches 3, 4 and 5 used for model making; batches 7, 8 and 9 used as external validation.

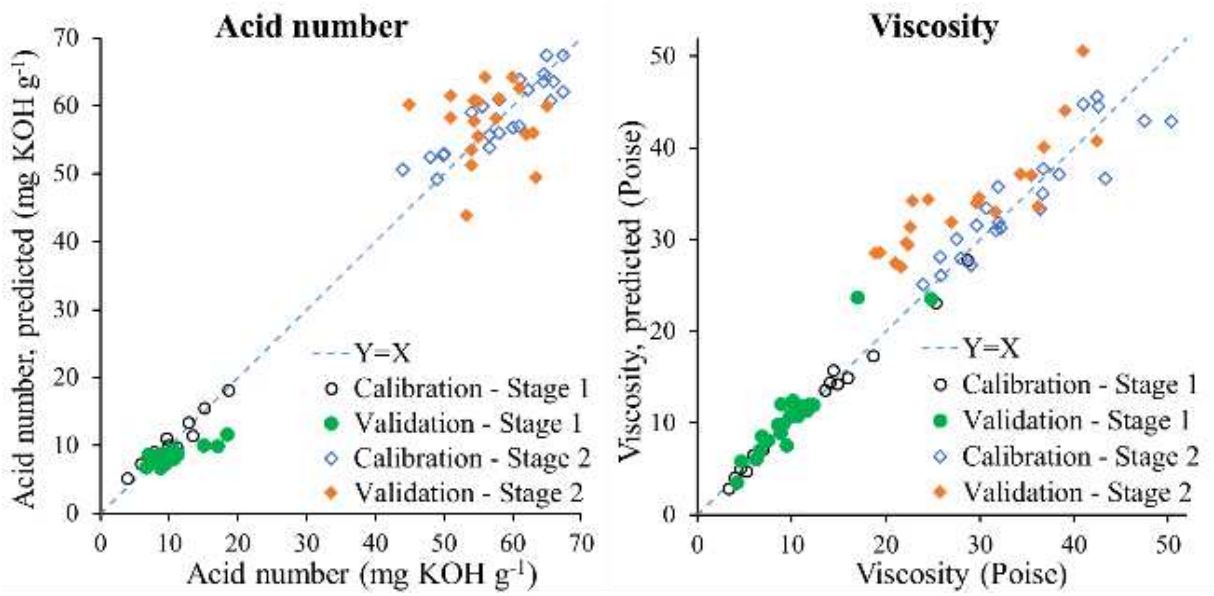

Fig. 6. Acid number and viscosity compared against NIR model predictions using calibration and validation batches for the two reaction stages.

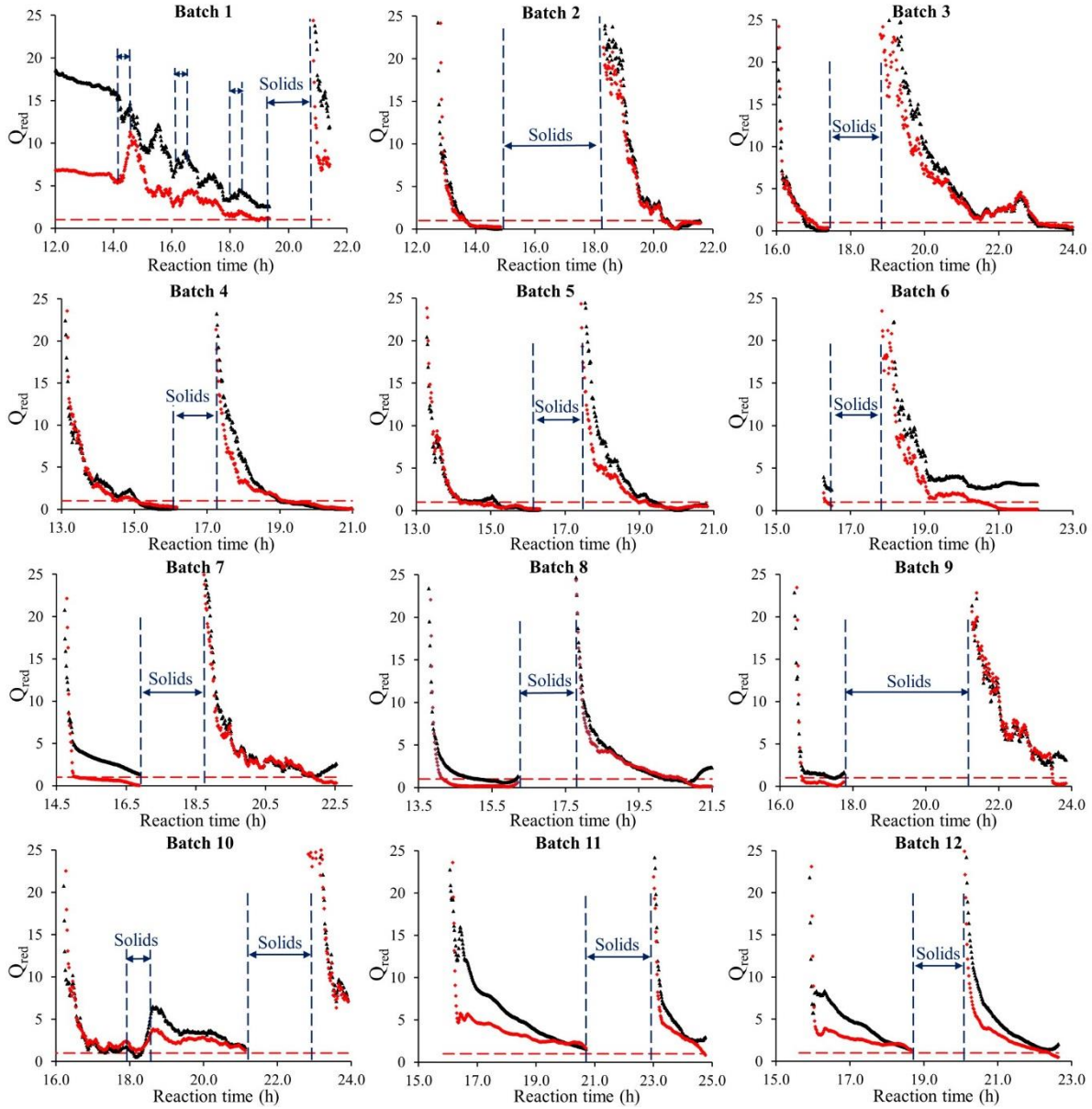

Fig. 7. PCA-based end-point detection MSPC Q_{red} charts predictions for all batches. Black dots indicate Q_{red} predictions from model developed using batches 2 to 5; red dots indicate Q_{red} predictions from updated model developed using batches 2 to 9; discontinuous red line indicates the end-point control limit.